Available online at www.sciencedirect.com
ScienceDirect
Journal of the European Ceramic Society 29 (2009) 1469–1476
www.elsevier.com/locate/jeurceramsoc

$LaGaO_3$-based cermet for solid oxide fuel cell cathodes

Pradyot Datta [a,c,*], Peter Majewski [b], Fritz Aldinger [c]

[a] Technische Universität Clausthal, Institut für Metallurgie, 42 Robert-Koch Strasse, Clausthal-Zellerfeld 38678, Germany
[b] University of South Australia, School of Advanced Manufacturing and Mechanical Engineering, Mawson Institute, Mawson Lakes, South Australia 5095, Australia
[c] Max-Planck-Institut für Metallforschung, Pulvermetallurgisches Laboratorium, Heisenbergstrasse 3, Stuttgart 70569, Germany

Received 15 June 2008; received in revised form 22 August 2008; accepted 28 August 2008
Available online 11 November 2008

Abstract

A series of $La_{0.9}Sr_{0.1}Ga_{0.85}Mg_{0.15}O_{3-\delta}$–Ag cermets with different Ag_2O contents were prepared by conventional sintering, assessing their suitability as cathode material for solid oxide fuel cell (SOFC) in combination with Sr- and Mg-doped $LaGaO_3$ electrolytes. Ag_2O is found to get dissociated at around 320 °C. The chemical compatibility between $La_{0.9}Sr_{0.1}Ga_{0.85}Mg_{0.15}O_{3-\delta}$–Ag (LSGM) and Ag was investigated by X-ray diffraction, scanning electron microscopy, transmission electron microscopy and X-ray photoelectron spectroscopy. No reaction or solid solubility between LSGM and Ag was found. Thermal expansion coefficients of the cermets were measured as a function of Ag content and were found to increase with increasing metallic content. Oxygen adsorption at the surface of the cermets could be detected.

Keywords: Oxide materials; Composite cathode; Thermal expansion; Photoelectron spectroscopies; X-ray diffraction

1. Introduction

Solid oxide fuel cell (SOFC) is an excellent system for generating electricity with high efficiency and little pollution. As a consequence oxygen conducting electrolyte materials are getting increasing attention. Among them, the solid electrolyte yttria stabilized zirconia (YSZ) has been most extensively studied. However, YSZ requires operation temperatures as high as about 1000 °C, which limits the field of application of SOFC based on this electrolyte. The main problems associated with high operating temperatures are prolonged start up time, problems with sealing, interconnect materials for SOFC stacks, thermal stresses at electrolyte–electrode interfaces, and interdiffusion between cell components.[1] Most of these problems will be minimized if the operating temperature of such systems can be lowered into the temperature range of around 600–800 °C.[2] A plethora of research activities were going on to find electrolyte materials with high oxygen ion conductivity in this temperature range. $LaGaO_3$, with a typical ABO_3 type structure, doped with Sr for A-site and Mg for B-site (LSGM), is one material that serves such needs.[3,4] However, to tap the potential of this material proper electrode materials need to be ensured. In this regard the selection of proper cathode materials is most significant. In comparison with the relatively fast H_2 oxidation reactions, polarization losses of O_2 (attributable to the high bond strength present in oxygen molecules) are particularly high due to the relatively high activation energy and consequently relatively slow reaction rates.[5–7] Thus, development of cathode materials with high electrocatalytic activity is critical in order to overcome the overpotential of the electrodes[8] in the temperature range of interest. Also the thermodynamic stability between the cathode and the electrolyte is of fundamental importance.[9]

Besides, materials for cathodes should have a high electronic conductivity for the transportation of electrons to the reaction site. Secondly, it needs to have high ionic conductivity for the transportation of the ions from the reaction site to the electrolyte. Finally, its microstructure should provide many contact points of reactive gas, electronic and ionic conductors (three phase boundary) in order to increase the number of electrochemically active sites.

Sr-doped $LaMnO_3$ (LSM) shows good electrode properties for YSZ electrolyte;[10] however, it becomes a poor electrode on LSGM due to a reaction between LSM and LSGM.[11–15]

* Corresponding author at: Technische Universität Clausthal, Institut für Metallurgie, 42 Robert-Koch Strasse, 38678, Clausthal-Zellerfeld, Germany. Tel.: +49 5323 723688; fax: +49 5323 723184.
E-mail address: pdatta@rediffmail.com (P. Datta).

0955-2219/$ – see front matter © 2008 Elsevier Ltd. All rights reserved.
doi:10.1016/j.jeurceramsoc.2008.08.030

Also, the oxygen ion conductivity of LSM materials and its oxygen trace diffusion coefficient is extremely low.[16,17] This poses practical limitations and restrictions to the application of LSM-based systems as potential cathodes for intermediate temperature SOFC.

$La_xSr_{1-x}Co_yFe_{1-y}O_{3-\delta}$ (LSCF) is a mixed electronic and ionic conductor. However, Dusastre and Kilner[18] reported that the ionic conductivity of this material drops rapidly with decreasing temperature, which eliminates this material for applications at temperatures below about 700 °C. Tanner et al.[19] used a model for describing the effect of porous composite electrodes on the overall charge-transfer process and predicted that composite electrodes could significantly improve the performance of fuel cells. Kenjo and Nishiya[20] showed that the overall polarization of the cathode can be lowered by using composite cathodes. Chen et al.[21,22] also found that the oxygen permeability of composite cathode materials is higher than that of pure oxides.

Recent results from literature[23–30] point out that a composite cathode consisting of silver as electronic conductor and a stabilized oxide phase as the ionic conductor exhibits outstanding performance compared to other frequently studied systems. The superior performance of the composite electrodes is attributed primarily to the fine-grained microstructure and high porosity of the composites as the ceramic phase hinders grain growth of silver phase in the composites.

In this paper attempts have been made to study LSGM–Ag cathode cermets for applications as cathode material for SOFCs based on LSGM electrolyte. The chemical compatibility between LSGM and Ag is investigated by means of scanning electron microscopy (SEM), energy dispersive X-ray analysis (EDX) and X-ray photo electron spectroscopy (XPS). Thermal expansion coefficient of LSGM–Ag cermets as a function of Ag content has also been determined.

2. Experimental procedure

The samples were prepared by solid state synthesis starting from powders of La_2O_3 (99.99%, Sigma–Aldrich, Steinheim, Germany) $SrCO_3$ (98%+, Sigma–Aldrich, Steinheim, Germany), Ga_2O_3 (99.99%, Sigma–Aldrich, Steinheim, Germany) and MgO (98%+, Merck, Darmstadt, Germany) details of which are given in another report.[31] Along with the powder of LSGM varying amounts of silver oxide (10–50 wt.%) were mixed separately and milled for 12 h in a zirconia ball mill to get a homogeneous mixture with a relatively small particle size. The homogenized powder mixtures were then isostatically cold pressed at 625 Mpa for 60 s into rectangular compacts with the dimensions of 15 mm × 5 mm × 5 mm. The pressed samples were then annealed at 600 °C for a duration of 20–100 h in static air atmosphere. The heating rate for all cases was 5 °C/min and all samples were furnace cooled to room temperature.

2.1. Sample characterization

The phase distributions of the calcined powders as well as sintered samples were studied by powder X-ray diffraction analysis (XRD) using Cu $K\alpha_{1+2}$ radiation with 40 kV acceleration voltage, 25 mA filament current (D5000, Kristalloflex, Siemens, Germany). The sample preparation was performed by crushing and grinding the compacts in an agate mortar, obtaining a fine-grained powder, which for XRD analysis was sprayed smoothly on a substrate. Diffraction data were smoothened and the background and Cu $K\alpha_2$ component were removed using the Siemens software package, DiffracAT, EVA5.0 rev.1.

Mean particle size of the powders and powder mixtures were measured in acetone medium in Mastersizer 2000 (Malvern Instruments Ltd., UK).

Microstructural characterization was performed by a scanning electron microscope (SEM Model REM S200, Cambridge Instruments, UK) using a Tungsten anode with an acceleration voltage of 20 kV. Chemical analysis was carried out on an attached EDX spectrometer (Model AN10000 pentafect detector, Link Systems, High Wycombe, UK). Specimens for SEM were prepared by embedding the samples in epoxy polymer and polishing with 1 μm diamond suspension on a soft polishing cloth (DP-NAP, Struers, Copenhagen, Denmark).

The theoretical density of the sintered samples was measured by Helium Pycnometry (Micromeritics, AccuPyc 1330, Australia), whereas the porosity was measured by conventional mercury porosimetry (Denver Instrument GmbH, Göttingen, Germany).

Linear thermal expansion coefficients of the samples were measured on samples which were annealed at 600 °C for 100 h. The measurement was carried out in air atmosphere using a push rod type differential dilatometer (Model 802, Bähr-Thermoanalyse GmbH, Hüllhorst, Germany) in the temperature range from room temperature to 900 °C. The reference sample used was a bar of sapphire of the dimension of 10 mm × 4 mm × 4 mm. Measurements were performed at a heating and cooling rate of 3 °C/min. Data acquisition of the differential length and temperature was conducted every second.

Differential scanning calorimetry (DSC) and thermogravimetric analysis (TG) (DSC/TG; Model STA 449C, NETZSCH-Gerätebau GmbH, Selb, Germany) were carried out using around 50 mg of powder sample in an alumina crucible up to 900 °C with a heating rate of 3 °C/min in argon atmosphere with 20% O_2.

Energy filtered transmission electron microscopy (EFTEM) was carried out using an instrument with a maximum acceleration voltage of 120 keV (Zeiss EM 912 Omega). The point resolution of this instrument is 3.8 Å.

X-ray photoelectron spectroscopy technique was employed to identify minute reactions between the ceramic phase and Ag. The XPS analysis was performed with a Thermo VG Thetaprobe system operating in the parallel data acquisition mode using monochromatic Al Kα ($h\nu = 1486.68$ eV; spot size 400 μm). Detail of the experimental set up is given elsewhere.[32]

For measuring the oxygen uptake and release of the perovskite during heat treatments the powder mixtures were analyzed with a Zeton Altamira AMI-200 catalyst characterization instrument. The experiments were carried out at ambient pressure in a quartz reactor using 200 mg of the powders.

Prior to the experiment, the powders were heated to 700 °C for 1 h in a flowing helium atmosphere with 7.5% oxygen to

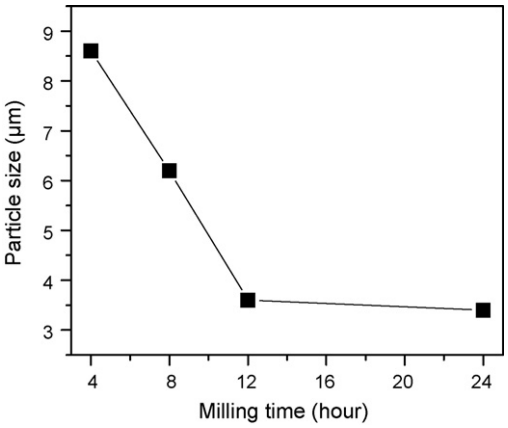

Fig. 1. Particle size variation of LSGM–30Ag_2O as a function of milling time.

remove any undesirable surface coverage (e.g. H_2O and CO_2). The temperature programmed reduction (TPR) and oxidation (TPO) cycles were conducted sequentially, each with a heating rate of 30 °C/min, a dwell time of 1 h at 700 °C and cooled down within approximately 30 min. All the steps of TPR and TPO cycles were conducted in the same gas (TPR: 100 ppm O_2 in He; TPO: 7.5% O_2 in He).

3. Results

3.1. Powder characterization

The average size of the LSGM and Ag_2O powder was measured and it is seen that average particle size of LSGM and Ag_2O are around 6 μm and 15 μm, respectively. The change of the mean particle size after milling of a mixture of LSGM with 30 wt.% Ag_2O is shown Fig. 1 as a function of milling time. After 12 h of milling there was little or no further reduction of the size of the particles. So, the powder mixtures which were milled for 12 h were taken for compaction and subsequent annealing.

3.2. Shrinkage behaviour

Differential thermal analysis studies were carried out for the green compacts of LSGM–10Ag_2O and LSGM–50Ag_2O and the results are shown in Fig. 2. Fig. 2A shows no indication

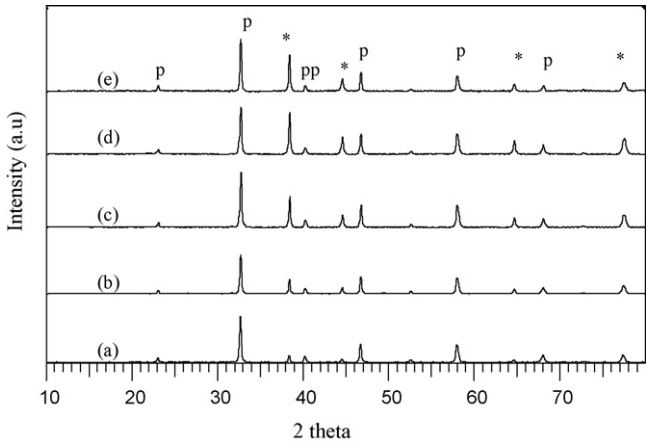

Fig. 3. XRD patterns of LSGM–Ag cermets after annealing at 600 °C for 100 h. (a)LSGM–10Ag_2O, (b) LSGM–20Ag_2O, (c) LSGM–30Ag_2O, (d) LSGM–40Ag_2O and (e) LSGM–50Ag_2O. (P = Perovskite, * = Ag).

of shrinkage up to 900 °C when the Ag_2O content is low but shrinkage is noticeable when the Ag_2O is as high as 50 wt.%. It is not surprising because Ag_2O gets dissociated at 320 °C. For comparison, the shrinkage behaviour of LSGM is also shown in Fig. 2B. It is noticed that the ceramic material does not experience any change in length up to a temperature of 1400 °C, and it undergoes sintering only at temperatures as high as 1450 °C.

3.3. XRD and SEM

LSGM–Ag_2O powder mixtures were compacted and annealed at 600 °C for 20 h, 60 h and 100 h. Phase evolution after annealing treatment was studied by X-ray diffraction method. Fig. 3 shows the XRD patterns after 100 h of annealing. The pattern reveals the presence of LSGM and Ag phases. It is interesting to note that there is no trace of any Ag_2O. Also, there is as such no qualitative difference of the phase mixture of the cermets irrespective of their starting Ag_2O contents. Quantitatively, 100% peak intensity of Ag which is observed at a 2θ value of 38.14° (JCPDS 89-3722) gets sharpened with the increase in the Ag_2O contents as can be seen by comparing the patterns in Fig. 3(a–e). SEM pictures of some of the cermets after 100 h of annealing are shown in Fig. 4. The dark phase is LSGM and the bright phase is Ag as identified by EDX analysis. The black

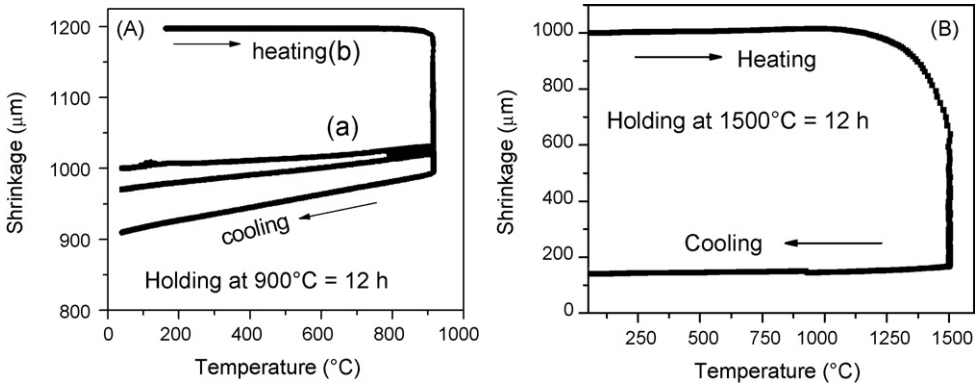

Fig. 2. (A) Shrinkage behaviour of LSGM–Ag_2O composites with temperature. (a) LSGM–10Ag_2O, (b) LSGM–50Ag_2O. (B) Shrinkage behaviour of LSGM.

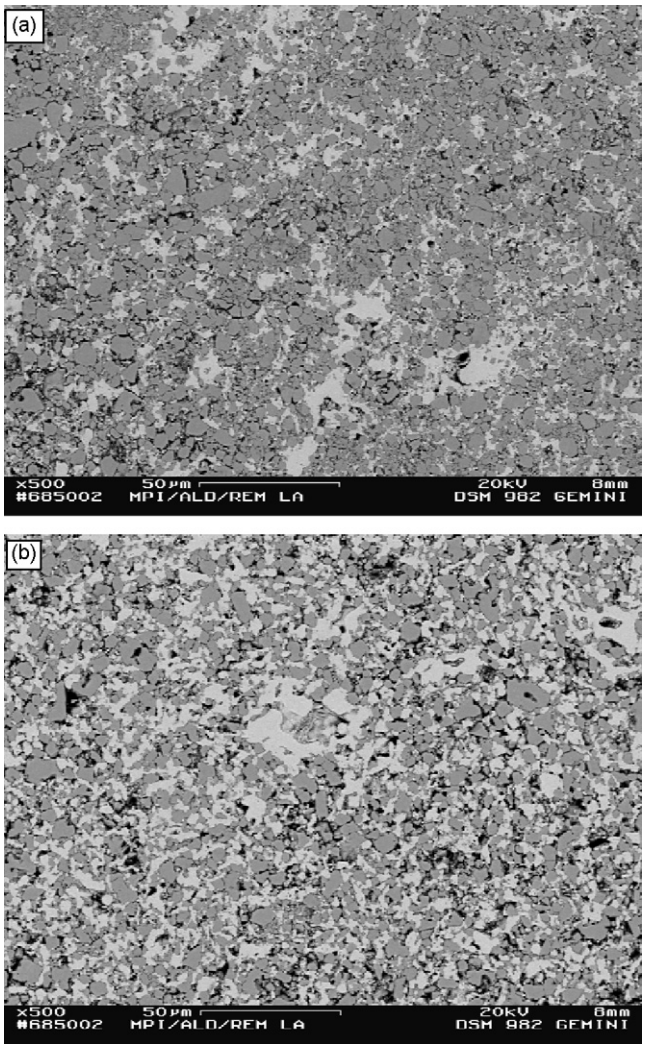

Fig. 4. SEM photographs of LSGM–Ag_2O cermets after annealing at 600 °C for 100 h. LSGM–30Ag_2O and (b) LSGM–50Ag_2O.

spots are porosities. Percolation of Ag in the ceramic phase is very clearly visible when Ag_2O content is minimum 30 wt.%. Mixture between the metal and ceramic phase is more intimate as the Ag_2O content is increased as can be seen by comparing Fig. 4 (a) and (b).

3.4. TEC

TEC values of the annealed Ag_2O born LSGM–Ag cermets were measured and are shown as a function of temperature in Fig. 5. All the cermets irrespective of their metallic contents show an increase in TEC with increasing temperature. Also, the higher is the amount of Ag_2O addition, the higher is the TEC at any given temperature.

3.5. Porosity

The theoretical density of LSGM was measured by Helium Pycnometry and was found to be 6.56 g/cm^3. The value of the same, calculated from the lattice parameters of LSGM (orthorhombic structure with $a = 5.5392$ Å, $b = 5.4975$ Å and

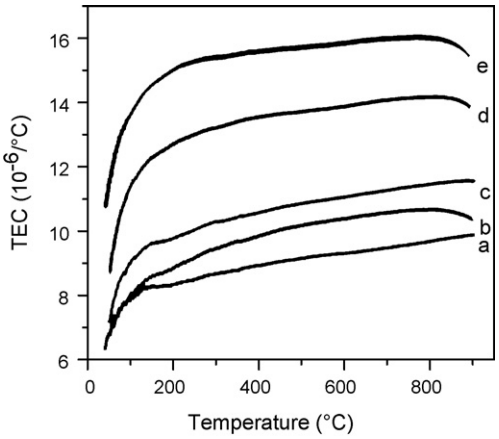

Fig. 5. Variation of TEC of LSGM–Ag_2O cermets with temperature. (a) LSGM–10Ag_2O, (b) LSGM–20Ag_2O, (c) LSGM–30Ag_2O, (d) LSGM–40Ag_2O, and (e) LSGM–50Ag_2O.

$c = 7.7484$ Å, $Z = 4$[33]) is found to be 6.8 g/cm^3. However, as the calculated value is for pure single phase LSGM and as the possibility of other phases present in LSGM cannot be ruled out, the measured value of LSGM is taken for further calculation. This is done for avoiding any over estimation of the porosity contents as the density of the normally present secondary phases like $LaSrGaO_4$ and $LaSrGa_3O_7$ are less than that of LSGM [$\rho LaSrGaO_4 = 6.39$ g/cm^3, $\rho LaSrGa_3O_7 = 5.56$ g/cm^3 [34]]. The theoretical density of silver is taken as 10.50 g/cm^3.[35] The density of the mixtures was calculated using the rule of mixture, i.e. assuming there is no interaction between the constituents of the mixtures. The variation of porosity of the cermets as a function of Ag_2O content is shown in Fig. 6. The figure indicates that the porosity increases as the Ag_2O content increases. This matches well with SEM photographs shown in Fig. 4. It is also noticed that there is very little variation of the porosity of the cermets with the change in annealing time as can be seen by comparing Fig. 6(a–c).

3.6. DSC and TGA

DSC and TG curves of the LSGM–50Ag_2O are shown in Fig. 7. The TG curve shows a loss of around 3% mass after

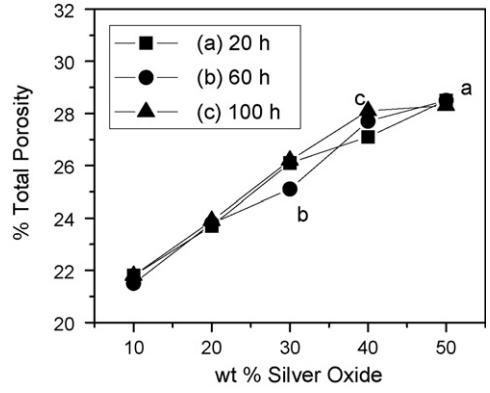

Fig. 6. Variation of porosity of LSGM with silver oxide after annealing at 600 °C for various durations in air.

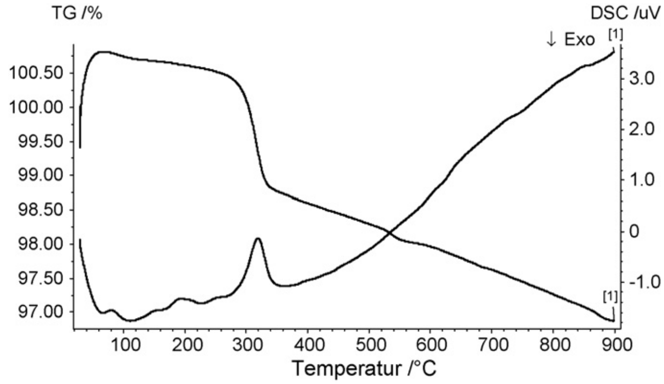

Fig. 7. DSC and TGA curves of LSGM–50Ag_2O up to 900 °C.

heating the sample up to 900 °C. It also shows a drop of about 2% mass sharply at around 320 °C. The corresponding DSC curve also shows an endothermic peak at the same temperature. No other significant change is observable in the curves.

3.7. TEM

A high resolution TEM picture of LSGM–30Ag_2O is shown in Fig. 8. No interdiffusion of LSGM or Ag is found. Interfacial phase formation is also not detected. From the EDX spectra it is noticed that Ag is present as metallic Ag.

3.8. X-ray photoelectron spectroscopy

The chemical state of the electrode surface was determined by XPS analysis. Core level spectra for the elements with highest photo ionization cross-section were only recorded. For example, Ag 3d has higher photo ionization cross-section value than Ag 4d. So, only the 3d peaks were recorded for extracting more reliable information. A general spectrum of Ag 3d peaks LSGM–30Ag_2O which were annealed for 100 h at 600 °C is given in Fig. 9.

3.9. TPR and TPO

Fig. 10A shows the oxygen release of LSGM with 30 wt.% Ag or Ag_2O as well as that of pure Ag_2O and LSGM. The figure clearly shows that with increasing temperature more and more oxygen is released from the cermets whereas the unmixed materials remain about the same throughout the entire treatment. Among the mixtures of LSGM, one with Ag_2O shows a little bit more release of oxygen than its Ag containing counterpart. The samples were cooled down to room temperature and then after changing the atmosphere to high oxygen partial pressure, the temperature was raised up to 700 °C. The corresponding TPO signals were measured and the result is shown in Fig. 10B. Virtually no difference other than the dissociation of Ag_2O is observed as can be seen by comparing the TPR and TPO curves.

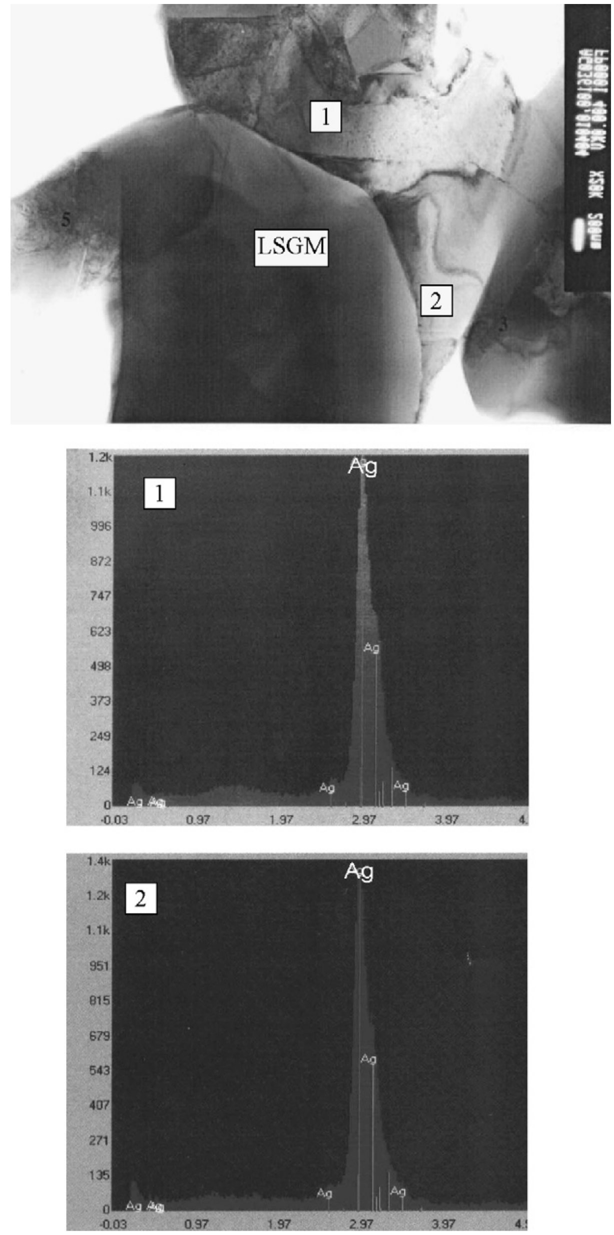

Fig. 8. TEM photograph and EDX spectra of LSGM–30Ag after annealing at 600 °C for 100 h.

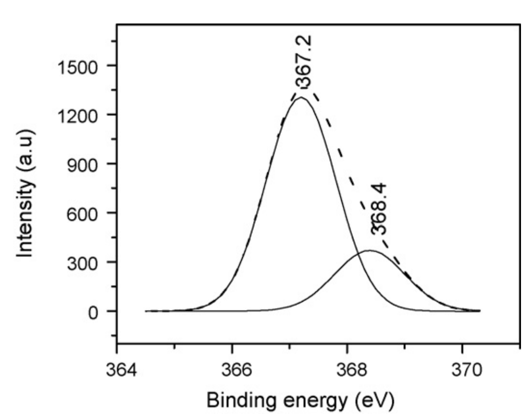

Fig. 9. Core level XPS spectra of Ag $3d_{5/2}$ from the surface and near surface region of a LSGM–30Ag_2O sample after annealing at 600 °C for 100 h.

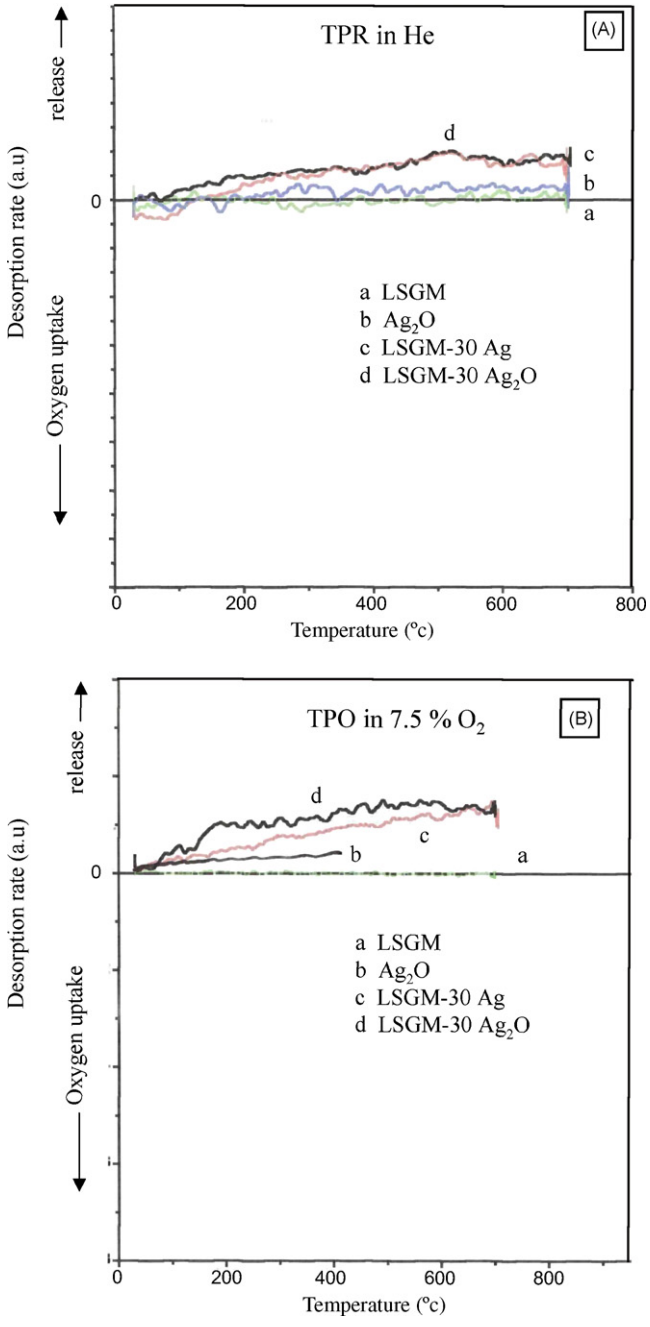

Fig. 10. (A) TPR and (B) TPO curves of LSGM and LSGM–Ag cermets.

4. Discussion

4.1. Interaction between LSGM and Ag

The annealing experiments reveal that LSGM does not interact with Ag irrespective of the silver content and the annealing time. XRD patterns taken at 600 °C and after an annealing time of even 100 h do not show any other phase beside LSGM and Ag. Thus, it can be conclusively said that metallic Ag and LSGM are chemically compatible. This result is somewhat expected since the radius of Ag^{2+} is 0.94 Å,[36] which is not favorable for forming solid solution with any of the constituent elements of LSGM as the radii are either too high (La^{3+} and Sr^{2+}) or too low (Ga^{3+} and Mg^{2+}), i.e. both differ by around 30–40%. TEM studies (Fig. 8) also confirm that there occurs no interfacial reaction during annealing of 100 h at 600 °C. Chemical reaction of Ag with La, Sr, Ga or Mg may not be possible because of the high cohesive energy of silver due to filled 4d electrons.[37]

4.2. Porosity

In the cermets Ag was added in oxide form and the porosity increases with increasing Ag_2O content (Fig. 6). This is because Ag_2O dissociates at around 320 °C and the degassing oxygen leaves behind porosity. The dissociation of Ag_2O is visible from the DSC curve of LSGM–50Ag_2O as has been shown in Fig. 7. The higher is the Ag_2O content, the higher is the weight loss and the increase in porosity. Similar results were observed with cermets prepared with gadolina doped ceria and silver oxide.[24]

4.3. TEC

TEC of a composite material is given by the following equation

$$\alpha_C = \alpha_A V_A + \alpha_B V_B$$

where V_i and α_i are volume fractions and TEC of the respective phases. As the TEC of silver is 19.1 $°C^{-1}$,[35] it is obvious from the above equation that with the increase of Ag_2O content the TEC of the LSGM–Ag_2O cermets will increase, as the latter gets dissociated to form Ag.

4.4. XPS

4.4.1. Ag 3d

There is a negative shift of Ag $3d_{5/2}$ of about 1 eV for the silver states of LSGM–30Ag_2O and also one additional peak is found at 368.4 eV. The high-energy peak is due to metallic silver. The low energy peak is due to the inducement of ionized silver atoms by adsorbed oxygen as the chemical characteristics of the adsorbed oxygen is of atomic in nature and of ionic in character like that of Ag–O bonding.[38] The adsorbed oxygen state can be related with that of surface oxide like film as proposed by Li et al.[39] When the electronic states of silver and oxygen overlap they will hybridize and form bonding and antibonding states. The hybridization energy will be attractive if only the bonding state becomes occupied, and it will counteract the energy loss due to orthogonalization. On the other hand, there will be no gain of energy due to hybridization if both bonding and antibonding states become occupied and the energy loss due to orthogonalization will prevail. Though earlier results indicate bulk nobleness of silver, but it seems the surface is not that noble. Normally, surface nobleness is determined by two factors. They are the degree of filling of the antibonding states on adsorption and the degree of orbital overlap with the adsorbate. Though Ag has a filled antibonding state[40] but as the orthogonalization energy cost is not much the net result of these two does not make the silver surface very noble and this is the reason for the adsorption of oxygen on the surface of silver.

It can be concluded that silver does not interact in any way with any constituent elements of LSGM other than the modification of the surface by adsorbing oxygen which is beneficial from the point of view of its catalytic activity.[39]

4.5. TPR and TPO

The oxygen stoichiometry varied depending upon the oxygen partial pressure of the atmosphere, temperature and the composition of the perovskite. If the conditions are changed part of the oxygen is released from or incorporated into the crystal lattice and can be obtained from TPR and TPO results. But, the release of oxygen from LSGM–Ag/Ag_2O mixture cannot be attributed to the release of lattice oxygen as LSGM does not change oxygen stoichiometry like Sr doped lanthanum cobaltate or lanthanum ferrate.[41] So, the release of oxygen is attributed to the release of oxygen adsorbed to the surface.[42] This is further substantiated from the TPO results (Fig. 10B). Had there been oxygen release during TPR from the lattice then during TPO one would have expected an absorption peak owing to oxygen uptake as the oxygen partial pressure in the latter experiment was kept high. But, no absorption peak is observed. Rather the same phenomenon as discussed above is noticed. Only cermet materials show the desorption of oxygen because of the catalytic activity of silver.[43]

5. Conclusion

In terms of chemical compatibility, thermal expansion coefficient values and porosity the cermet materials based on LSGM and Ag seem to fulfil all the criteria for the usage as cathode materials for SOFC. Varying the amount of metallic content, its percolating limit has also been ascertained. However, further detailed electrochemical studies are needed to be done with the cermets. The cermet materials can be a good choice for the preparation of cathode supported cells.

Acknowledgements

Financial support from the Deutsche Forschungsgemeinschaft (DFG) for carrying out this work is gratefully acknowledged. The authors would also like to thank Dr. A. Mai of Forschungszentrum Jülich, Germany, for carrying out the TPR and TPO experiments.

References

1. Steele, B. C. H. and Heinzel, A., Materials for fuel cell technologies. *Nature*, 2001, **414**, 345–352.
2. Doshi, R., Richards, V. L., Carter, J. D., Wang, X. P. and Krumpelt, M. R., Development of solid-oxide fuel cells that operate at 500 °C. *J. Electrochem. Soc.*, 1999, **146**(4), 1273–1278.
3. Ishihara, T., Matsuda, H. and Takita, Y., Doped-$LaGaO_3$ perovskite type oxide as a new oxide ionic conductor. *J. Am. Chem. Soc.*, 1994, **116**, 3801–3803.
4. Feng, M. and Goodenough, J. B., A superior oxide ion electrolyte. *Eur. J. Solid State Inorg. Chem.*, 1994, **31**, 663–672.
5. Jiang, S. P. and Badwal, S. P. S., An electrode kinetics study of H oxidation on Ni/Y_2O_3–ZrO_2 cermet electrode of the solid oxide fuel cell. *Solid State Ionics*, 1999, **123**, 209–224.
6. Jiang, S. P., Love, J. G. and Ramprakash, Y., Electrode behaviour at (La, Sr)MnO_3/Y_2O_3–ZrO_2 interface by electrochemical impedance spectroscopy. *J. Power Sources*, 2002, **110**, 201–208.
7. Fleig, J., SOFC cathodes: polarization mechanisms and modelling of the electrochemical performance. *Annu. Rev. Mater. Res.*, 2003, **33**, 361–382.
8. Endo, A., Fukunaga, H., Wen, C. and Yamada, K., Cathodic reaction mechanism of dense $La_{0.6}$ $Sr_{0.4}CoO_3$ and $La_{0.81}Sr_{0.09}MnO_3$ electrodes for solid oxide fuel cells. *Solid State Ionics*, 2000, **135**, 353–358.
9. van Roosmalen, J. A. M. and Cordfunke, E. H. P., Chemical reactivity and interdiffusion of (La, Sr)MnO_3 and (Zr, Y)O_2, solid oxide fuel cell cathode and electrolyte materials. *Solid State Ionics*, 1992, **52**, 303–312.
10. Tsai, T. and Barnet, S. A., Effect of LSM–YSZ cathode on thin-electrolyte solid oxide fuel cell performance. *Solid State Ionics*, 1997, **93**, 207–217.
11. Yi, J. Y. and Choi, G. M., Cathodic properties of $La_{0.9}Sr_{0.1}MnO_3$ electrode for fuel cells based on $LaGaO_3$ solid electrolyte. *J. Eur. Ceram. Soc.*, 2004, **24**, 1359–1363.
12. Huang, K. and Goodenough, J. B., A solid oxide fuel cell based on Sr- and Mg-doped $LaGaO_3$ electrolyte: the role of a rare-earth oxide buffer. *J. Alloys Compd.*, 2000, **303–304**, 454–464.
13. Huang, K., Feng, M., Goodenough, J. B. and Schmerling, M., Characterization of Sr-doped $LaMnO_3$ and $LaCoO_3$ as cathode materials for a doped $LaGaO_3$ ceramic fuel cell. *J. Electrochem. Soc.*, 1996, **143**, 3630–3636.
14. Rozumek, M., Majewski, P., Maldener, T. and Aldinger, F., Study of the solid state reactions between (La, Sr) (Ga, Mg)O_3 and (La, Sr)MnO_3, (La, Ca)CrO_3 and Ni. *Mat-wiss. u. Werkstofftech*, 2002, **33**, 348–354.
15. Yi, J. Y. and Choi, G. M., The effect of mixed conductivity on the cathodic overpotential of $LaGaO_3$-based fuel cell. *Solid State Ionics*, 2004, **175**, 145–149.
16. Carter, S., Selcuk, A., Chater, R. J., Kajda, J., Kilner, J. A. and Steele, B. C. H., Oxygen transport in selected nonstoichiometric perovskite-structure oxides. *Solid State Ionics*, 1992, **53–56**, 597–605.
17. De Souza, R. A., Kilner, J. A. and Walker, J. F., A SIMS study of oxygen tracer diffusion and surface exchange in $La_{0.8}Sr_{0.2}MnO_{3+\delta}$. *Mater. Lett.*, 2000, **43**, 43–52.
18. Dusastre, V. and Kilner, J. A., Optimisation of composite cathodes for intermediate temperature SOFC applications. *Solid State Ionics*, 1999, **126**, 163–174.
19. Tanner, C. W., Fung, K. Z. and Virkar, A. V., The effect of porous composite electrode structure on solid oxide fuel cell performance. *J. Electrochem. Soc.*, 1997, **144**, 21–30.
20. Kenjo, T. and Nishiya, M., $LaMnO_3$ air cathodes containing ZrO_2 electrolyte for high temperature solid oxide fuel cells. *Solid State Ionics*, 1992, **57**, 295–302.
21. Chen, C. S., Kruidhof, H., Bouwmeester, H. J. M., Verweij, H. and Burggraff, A. J., Oxygen permeation through oxygen ion oxide-noble metal dual phase composites. *Solid State Ionics*, 1996, **86–88**, 569–572.
22. Chen, C. S., Boukamp, B. A., Bouwmeester, H. J. M., Gao, G. Z., Kruidhof, H., Winnbust, A. J. A. *et al.*, Microstructural development, electrical properties and oxygen permeation of zirconia–palladium composites. *Solid State Ionics*, 1995, **76**, 23–28.
23. Wang, L. S. and Barnett, S. A., Ag–perovskite cermets for thin film solid oxide fuel cell air-electrode applications. *Solid Sate Ionics*, 1995, **76**, 103–113.
24. Datta, P., Majeski, P. and Aldinger, F., Synthesis and characterization of gadolinia doped ceria–silver cermet cathodes for solid oxide fuel cell. *Mater. Chem. Phys.*, 2008, **107**, 370–376.
25. Hu, H. and Liu, M., Silver–$BaCe_{0.8}Gd_{0.2}O_3$ composites as cathode materials for SOFCs using $BaCeO_3$-based electrolytes. *J. Electrochem. Soc.*, 1996, **143**, 859–864.
26. Wu, Z. L. and Liu, M., Ag–$Bi_{1.5}Y_{0.5}O_3$ composite cathode materials for $BaCe_{0.8}Gd_{0.2}O_3$-based solid oxide fuel cells. *J. Am. Ceram. Soc.*, 1998, **81**, 1215–1220.
27. Xia, C., Zhang, Y. and Liu, M., A composite cathode based on yttria stabilized bismuth oxide for low-temperature SOFCs. *Appl. Phys. Lett.*, 2003, **82**, 901–903.
28. Xia, C. and Liu, M., Novel electrode materials for low-temperature solid oxide fuel cells. *Adv. Mater.*, 2002, **14**, 521–523.

29. Camaratta, M. and Wachsman, E., Silver–bismuth oxide cathodes for IT-SOFCs. Part II. Improving stability through microstructural control. *Solid State Ionics*, 2007, **178**, 1411–1418.
30. Jaiswal, A. and Wachsman, E. D., Direct current bias studies on $(Bi_2O_3)_{0.8}(Er_2O_3)_{0.2}$ electrolyte and Ag–$(Bi_2O_3)_{0.8}(Er_2O_3)_{0.2}$ cermet electrode. *Solid State Ionics*, 2006, **177**, 677–685.
31. Datta, P., Majewski, P. and Aldinger, Synthesis and characterization of Sr and Mg substituted $LaGaO_3$–nickel cermet anode for solid oxide fuel cell. *Mater. Chem. Phys.*, 2007, **102**, 125–131.
32. Datta, P., Majewski, P. and Aldinger, X-ray photoelectron spectroscopic study of Sr and Mg doped $LaGaO_3$ solid electrolyte surface. *Mater. Res. Bull.*, 2008, **43**, 1–8.
33. Datta, P., Majewski, P. and Aldinger, F., Structural studies of Sr- and Mg-doped $LaGaO_3$. *J. Alloy. Compds.*, 2007, **438**, 232–237.
34. Khanlou, A. A., Tietz, F. and Stöver, D., Material properties of $La_{0.8}Sr_{0.2}Ga_{0.9+x}Mg_{0.1}O_{3-\delta}$ as a function of Ga content. *Solid State Ionics*, 2000, **135**, 543–547.
35. Smithells, C. J. and Brandes, E. A., ed., *Metals Reference Book*. 5th edition Butterworths, London and Boston, 1976.
36. Shannon, R. D., Revised effective ionic radii and systematic studies of interatomic distances in halides and chalcogenides. *Acta Crystall. A*, 1976, **32**, 751–767.
37. Tjeng, L. H., Meinders, M. B. J., Van Elp, J., Ghijsen, J. and Sawatzky, G. A., Electronic structure of Ag_2O. *Phys. Rev. B*, 1990, **41**, 3190–3199.
38. Boronin, A. I., Koscheev, S. V. and Zhidomirov, G. M., XPS and UPS study of oxygen states on silver. *J. Electron Spectrosc. Relat. Phenom.*, 1998, **96**, 43–51.
39. Li, W. X., Stampfl, C. and Scheffler, M., Why is a noble metal catalytically active? The role of the O–Ag interaction in the function of silver as an oxidation catalyst. *Phys. Rev. Lett.*, 2003, **90**, 256102-1–256102-4.
40. Hammer, B. and Norskov, J. K., Why gold is the noblest of all the metals. *Nature*, 1995, **376**, 238–240.
41. Mai, A., Tietz, F. and Stöver, D., Partial reduction and re-oxidation of iron- and cobalt-containing perovskites using catalyst characterisation measurements. *Solid State Ionics*, 2004, **173**, 35–40.
42. Chan, K. S., Ma, J., Jaenicke, S., Chuah, G. K. and Lee, J. Y., Catalytic carbon monoxide oxidation over strontium, cerium and copper-substituted lanthanum manganates and cobaltates. *Appl. Catal. A.*, 1994, **107**, 201–227.
43. Liu, M. and Wu, Z., Significance of interfaces in solid-state cells with porous electrodes of mixed ionic–electronic conductors. *Solid State Ionics*, 1998, **107**, 105–110.